

## Direct Imaging of Interfacial Ordering in Ultrathin $(\text{Si}_m\text{Ge}_n)_p$ Superlattices

D. E. Jesson and S. J. Pennycook

*Solid State Division, Oak Ridge National Laboratory, Oak Ridge, Tennessee 37831*

J.-M. Baribeau

*Institute for Microstructural Sciences, National Research Council of Canada, Ottawa, Canada K1A 0R6*

(Received 8 August 1990; revised manuscript received 21 November 1990)

We present the first atomic-resolution images of interfacial ordering occurring in ultrathin  $(\text{Si}_m\text{Ge}_n)_p$  superlattices. The observed asymmetric interfacial abruptness is associated with several distinct ordered configurations, which differ from phases considered previously. This is explained by a novel Ge-atom pump mechanism which is chemically driven, and takes place principally at the rebonded edge configuration during type- $S_B$  step propagation, leading to lateral  $(2 \times 2)$  compositional ordering.

PACS numbers: 68.65.+g, 61.16.Di

The growth of ultrathin  $(\text{Si}_m\text{Ge}_n)_p$  superlattices by molecular-beam epitaxy (MBE) is currently receiving considerable attention.<sup>1</sup> The aim is to produce a direct- or quasidirect-band-gap material as a result of zone-folding effects which, if realized, could dramatically advance the integration of optoelectronics with Si-based technologies.<sup>2,3</sup> However, recent diffraction evidence<sup>4</sup> for the occurrence of interfacial ordering in these systems has important implications for both band-structure calculations and the physical properties of the superlattice itself. Presently, critical questions concerning the origin, structure, and morphology of the ordered phase as well as its relationship to growth conditions remain completely unanswered. Selected-area electron diffraction has become the standard approach for identifying additional periodicities occurring in multilayer systems. However, beyond inferring the presence or absence of ordering the quantitative value of the technique is extremely limited. Superlattice spot intensities are complicated by orientational and thickness averaging, the presence of twins and antiphase domain boundaries, as well as single scattering from Bloch states of the parent lattice. Furthermore, all experimental observations to date<sup>4,5</sup> have been interpreted only in terms of the two model structures which have so far been proposed.<sup>6,7</sup> In this Letter, we apply a fundamentally different approach to the study of interfacial ordering based on  $Z$ -contrast scanning transmission electron microscopy (STEM).<sup>8</sup> Using this direct imaging technique we show for the case of superlattices that the ordered phase does not correspond to either proposed structure and can, in fact, take different forms at neighboring superlattice interfaces. These forms can be explained by a novel Ge-atom pump mechanism which is intrinsically linked to the  $(2 \times 1)$  reconstructed surface and occurs specifically at the rebonded edge configuration during monolayer step growth.

The  $Z$ -contrast technique has been described in detail in a number of recent publications.<sup>8,9</sup> Here we simply list the salient features of the approach which are directly relevant to the atomic imaging of  $(\text{Si}_m\text{Ge}_n)_p$  superlat-

tices. Briefly, a coherent electron probe of diameter 2.2 Å (FWHM intensity) is scanned over a thin specimen. Simultaneously, transmitted electrons scattered through large angles are collected by an annular detector so that a map of the specimen scattering power is built up. For the [110] projection consisting of an arrangement of pairs of atoms or dumbbells separated by a distance of 1.36 Å, the 2.2-Å probe will resolve individual dumbbells but not the atoms comprising the dumbbells. Each bright spot or column in the  $Z$ -contrast image therefore corresponds to an individual atomic dumbbell and is slightly elongated along [001] as expected. The column positions are independent of objective-lens defocus and specimen thickness. Most importantly, there are no Fresnel interference effects at the multilayer boundaries to obscure interfacial ordering. Finally, Bloch-wave calculations show that, to within 10%, the scattering power of each atomic column is proportional to the large-angle columnar scattering cross section which approaches the atomic-number-squared ( $Z^2$ ) dependence of nuclear Rutherford scattering.<sup>10</sup> Thus, a  $Z$ -contrast image represents an intuitively interpretable atomic-scale map of the structure and chemistry of the superlattice projection.

In Fig. 1 we show a  $Z$ -contrast image of a  $(\text{Si}_4\text{Ge}_8)_{24}$  superlattice which represents the first direct image of ordering in the Si-Ge system. Remarkably, three distinct types of interfacial ordering can be identified. A strong  $(2 \times n)$  periodicity is apparent in the topmost deposited Si layer, alternate  $\langle 111 \rangle$  planar ordering in the central Si layer, and crosslike structures in the bottom Si layer. Such features have been consistently observed in all of our images to date. The ordering is predominantly confined to the Si layers and is accompanied by an asymmetric interfacial abruptness in which the Si-on-Ge interface is less abrupt than the Ge-on-Si interface. These results clearly and unambiguously demonstrate that the situation is in fact far more complicated than previously imagined.

We now propose a novel Ge-atom pump mechanism

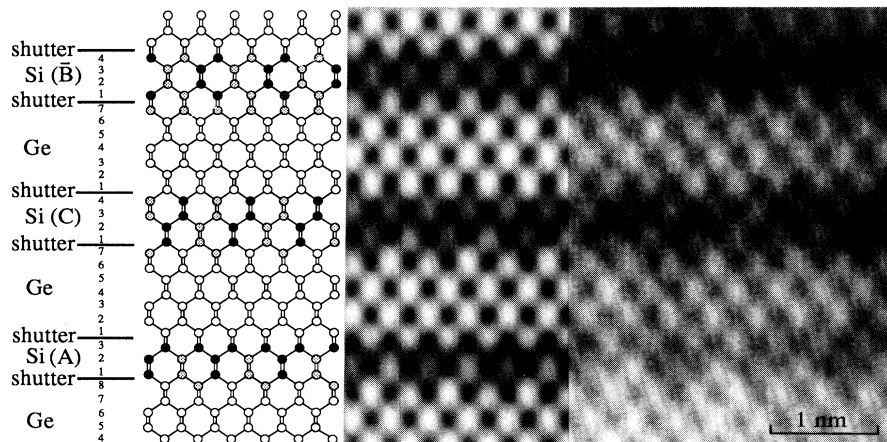


FIG. 1. [110] Z-contrast STEM image of a nominal  $(\text{Si}_4\text{Ge}_8)_{24}$  superlattice showing interfacial ordering. The [001] growth direction is toward the top of the image with the sample thickness increasing toward the lower left-hand corner. Our interpretation of the superlattice structure based on the image simulation indicates the sequential deposition of Si and Ge layers together with the ordered structures  $\bar{B}$ , C, and A resulting from the atom pump mechanism. Open circles represent Ge columns; solid circles, Si columns; and shaded circles, alloy columns. Simulation parameters are  $C_s = 1.3$  mm, convergence angle = 10.3 mrad, and defocus =  $-69.4$  nm.

which accounts for all of the various image forms and also explains the asymmetric interfacial abruptness. The superlattice shown in Fig. 1 was grown by MBE directly onto a Ge substrate at  $350^\circ\text{C}$  with a deposition rate of  $0.5 \text{ \AA s}^{-1}$ .<sup>11</sup> The presence of significant quantities of Ge in the Si layers is therefore of considerable surprise for such low-temperature growth. Strain-enhanced interdiffusion of Ge into Si is expected to be small or negligible at this growth temperature<sup>12</sup> and the alternative explanation of Ge islanding during growth can be immediately ruled out from the compositional uniformity of our images. At low temperatures the surface diffusion lengths are considerably smaller than the typical distance between steps so that growth occurs via monolayer-height island formation and the consecutive interchange of  $(2 \times 1)$  and  $(1 \times 2)$  domains.<sup>13</sup> At  $350^\circ\text{C}$  this process is strongly anisotropic with a preferred growth direction perpendicular to the dimer rows of the original surface reconstruction. Two-dimensional island growth therefore proceeds via the formation and propagation of  $S_B$ -type single-layer steps in the notation of Chadi.<sup>14</sup> Consider a single dimer string (or an island several dimers wide) growing along  $[1\bar{1}0]$ . Silicon atoms diffusing to the rebonded step edge in Fig. 2(a) will break Ge dimer bonds to form the Si dimer pair of Fig. 2(b). The relaxation of appreciable bond-length strain is, however, negated by the presence of unsaturated bonds at the step edge, so that this step is energetically unfavorable compared with the rebonded structure in Fig. 2(a). We now examine suitable candidate sites for a possible adatom-substrate exchange mechanism driven by total-energy minimization. At low growth temperatures, exchange paths involving tetrahedrally coordinated subsurface sites will be kinetically frozen, even in the proximity of the  $(2 \times 1)$  reconstruction. A more likely possibility is

the interchange of relatively weakly bound nearest-neighbor atoms at the step edge. We note, however, that an interchange of Si and Ge atoms at the step edge in Fig. 2(b) will not significantly affect the strain energy or reduce the number of unsaturated bonds, so that this

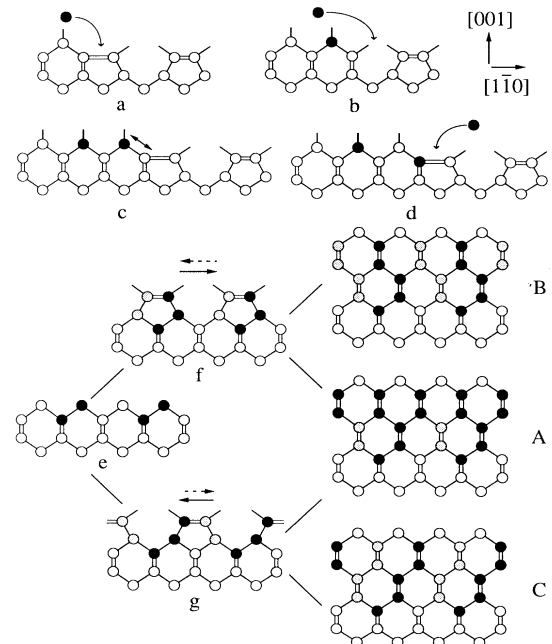


FIG. 2. Growth kinetics model for Ge segregation and ordering resulting from Si deposition on a  $(2 \times 1)$  reconstructed surface. Open circles represent Ge columns; solid circles, Si columns; and shaded circles, alloy columns. The exchange arrowed in (c) replaces a Si surface dangling bond with a Ge dangling bond (d).

configuration remains stable during growth. The next pair of Si atoms growing at this step edge [Fig. 2(c)] are, however, unstable compared with the interchange of Si and Ge edge atoms [Fig. 2(d)], which replaces a Si surface dangling bond by a Ge dangling bond. We estimate a driving force of the order 0.45 eV per exchange from the energy difference between unsaturated Si and Ge bonds and the replacement of a homopolar Ge bond with a Si-Ge heteropolar bond.<sup>15</sup> In this sense, the  $(2\times 1)$  surface reconstruction and in particular the rebonded edge-step configuration acts as a chemically driven atom pump for Ge segregation. As in Fig. 2(a), the next Si-atom pair will assume a stable configuration. This asymmetric pumping mechanism therefore configures the dimer string(s) into alternating Si and Si-Ge alloy columns as growth proceeds along  $[1\bar{1}0]$  [Fig. 2(e)]. Since each island appears to nucleate independently, coalescence into larger islands will be accompanied by the formation of antiphase boundaries between translationally inequivalent  $(2\times 1)$  domains.<sup>13</sup> The intrinsically small domain size associated with low-temperature epitaxy will therefore also restrict the lateral extent of the ordered domains, which is in excellent agreement with our observations.

The next monolayer of Si growth occurs via  $(2\times 1)$  domains and  $S_B$  steps with the dimer rows parallel to  $[110]$ . The Ge-atom pump mechanism [Figs. 2(a)-2(e)] can only operate selectively on the alloy columns, giving rise to the translationally inequivalent ordered structures shown in Figs. 2(f) and 2(g). Since the surface dimerization is only weakly influenced by subsurface strain, at low temperatures we would expect both configurations to occur. The next monolayer of Si growth will repeat steps 2(a)-2(e) although the growth direction is now critical to the nature of the ordered phase and three distinct possibilities exist. First, consider  $S_B$ -type step propagation along the  $\langle 110 \rangle$  directions shown by the dashed arrows in Figs. 2(f) and 2(g). This will avoid the unstable step configuration shown in Fig. 2(c) and terminate the atom pump mechanism to produce the interfacial  $(2\times 2)$  reconstruction labeled as structure *A*. Monolayer step growth along the  $\langle 110 \rangle$  direction indicated by the solid arrow in Fig. 2(f) results in a second structure *B* showing a reversal in the ordering direction. Finally, monolayer step propagation in the direction of the solid arrow in Fig. 2(g) produces the five-monolayer-ordered configuration labeled as structure *C*. This structure is similar to a  $[110]$  projection of ordering on alternate  $\{111\}$  planes as described by Littlewood.<sup>7</sup> However, our interfacial phase differs from the Littlewood structure in that similar  $\langle 111 \rangle$  ordering along the orthogonal  $[1\bar{1}0]$  projection is predicted. Three additional structures  $\bar{A}$ ,  $\bar{B}$ , and  $\bar{C}$  can be generated by applying the model of Fig. 2 to a substrate having one additional Ge monolayer and are equivalent to viewing structures *A*, *B*, and *C* along the  $[1\bar{1}0]$  direction.<sup>16</sup>

All ordered configurations are also accompanied by a compositional modulation along the growth direction. Defining  $\alpha$  as the fraction of available Ge atoms which are propagated to the surface layer by our pump mechanism during each growth step, it is possible to generate the composition gradient from our model and perform the corresponding *Z*-contrast image simulations.<sup>8-10</sup> We find excellent agreement between the ordering in the top-most deposited Si layers and structure  $\bar{B}$  for  $\alpha=0.75$ . Careful examination of the columnar intensities eliminates the orthogonal projection (structure *B*) so that by computer simulation it is possible to deduce precisely how the superlattice has grown in this region, i.e., that Si deposition began on a Ge  $(1\times 2)$  domain. Similar considerations identify the central and lower ordered regions in Fig. 1 with structures *C* and *A*, respectively. We emphasize that clear projections of structures *A-C* are only attainable in very-thin-crystal regions ( $\lesssim 5$  nm) since in thicker samples several domains will be sampled in projection.

We now consider the important implications of our model for the growth of high-quality ultrathin  $(\text{Si}_m\text{Ge}_n)_p$  superlattices. Assuming  $\alpha$  has the usual Arrhenius hopping form, the Ge concentration profiles shown in Fig. 3 for structure *C* can be interpreted as the temperature dependence of the pumping mechanism. At very low temperatures, just above the crystalline-amorphous transition range, we would expect the pumping action of the rebonded edge-step configuration to be kinetically frozen as suggested by the  $\alpha=0.25$  curve. Low-temperature growth at around 250°C followed by rapid thermal annealing may therefore favor the generation of abrupt structures as suggested by Iyer *et al.*<sup>17</sup> At much higher growth temperatures, approximated by  $\alpha=1$ , our model predicts the formation of a Ge-rich adlayer floating on the growing Si layer. The net result is strong ordering confined to bilayer and monolayer regions at the two interfaces but with no ordering present in the intervening Si layer. However, this discrete interfacial order-

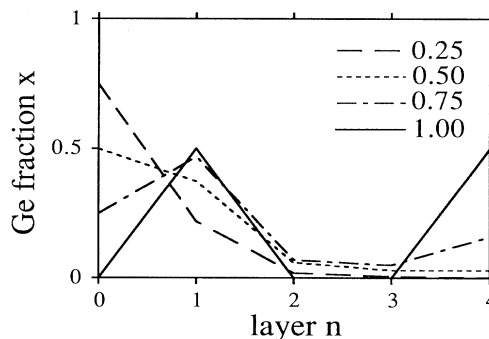


FIG. 3. Ge fraction  $x$  for alloy columns in the  $n$ th deposited Si layer as a function of the adatom-substrate exchange parameter  $\alpha$ .

ing would presumably be destroyed by strain-enhanced interdiffusion at such high growth temperatures. At intermediate growth temperatures (300–400°C) our pump mechanism will result in appreciable ordering over five monolayers as observed experimentally. The build up of Ge in the fourth layer of Fig. 3 is a result of pumped Ge being dumped when the Ge shutter is opened and a low-energy Ge surface is deposited in the fifth layer. The fourth-layer Ge concentration is, however, significantly smaller than the first-layer concentration which is the origin of the asymmetric interfacial abruptness observed in our images. Observation of an asymmetric Ge distribution in  $(\text{Si}_m\text{Ge}_n)_p$  multilayers has also been made using Raman spectroscopy.<sup>17</sup> In this work the authors clearly appreciated the important role of the free surface during growth but did not specifically consider the  $(2\times 1)$  reconstruction and monolayer step growth. Our model, therefore, provides a clear, atomistic picture of Ge segregation and for the first time links the effect with  $\langle 111 \rangle$  ordering.<sup>18</sup> To obtain abrupt interfaces in this important temperature regime it would therefore seem necessary to destroy the  $(2\times 1)$  reconstruction. In this regard, the use of an Sb passivating layer has already proved successful for the MBE growth of alloy layers.<sup>19</sup> Other techniques such as chemical vapor deposition may not involve the  $(2\times 1)$  reconstruction and result in sharper interfaces without ordered phases. We also note that the degree of Ge segregation into the Si layer may also be sensitive to the Si deposition rate so that higher rates (within the limits imposed by surface roughening) could improve the interface quality. More generally, if the growth kinetics can be controlled in this temperature regime, surface reconstructions may facilitate the design of novel 3D-ordered architectures with greatly modified band structures. With passivating layers, such structures might even include the growth of ordered-disordered multilayers.

This research was sponsored by the Division of Materials Science, U.S. DOE under Contract No. DE-AC05-84OR21400 with Martin Marietta Energy Systems, Inc. and in part by an appointment to the U.S. DOE Postgraduate Research Program administered by Oak Ridge Associated Universities.

<sup>1</sup>See, for example, *Thin Solid Films* **183** (1989).

<sup>2</sup>S. Froyen, D. M. Wood, and A. Zunger, *Phys. Rev. B* **36**,

4547 (1987).

<sup>3</sup>T. P. Pearsall *et al.*, *Phys. Rev. Lett.* **58**, 729 (1987).

<sup>4</sup>E. Müller, H.-U. Nissan, M. Ospelt, and H. von Känel, *Phys. Rev. Lett.* **63**, 1819 (1989).

<sup>5</sup>F. K. LeGoues, V. P. Kesan, and S. S. Iyer, *Phys. Rev. Lett.* **64**, 40 (1990).

<sup>6</sup>A. Ourmazd and J. C. Bean, *Phys. Rev. Lett.* **55**, 765 (1985).

<sup>7</sup>P. B. Littlewood, *Phys. Rev. B* **34**, 1363 (1986).

<sup>8</sup>S. J. Pennycook and D. E. Jesson, *Phys. Rev. Lett.* **64**, 938 (1990).

<sup>9</sup>D. E. Jesson, S. J. Pennycook, and M. F. Chisholm, *Mater. Res. Soc. Symp. Proc.* **159**, 439 (1990); S. J. Pennycook, D. E. Jesson, and M. F. Chisholm, *Mater. Res. Soc. Symp. Proc.* **183**, 211 (1990).

<sup>10</sup>D. E. Jesson, S. J. Pennycook, and J.-M. Baribeau, *Mater. Res. Soc. Symp. Proc.* **183**, 223 (1990).

<sup>11</sup>J.-M. Baribeau *et al.*, *J. Vac. Sci. Technol. A* **5**, 1898 (1987).

<sup>12</sup>G. L. McVay and A. R. DuCharme, *J. Appl. Phys.* **44**, 1409 (1973).

<sup>13</sup>R. J. Hamers, U. K. Köhler, and J. E. Demuth, *J. Vac. Sci. Technol. A* **8**, 195 (1990).

<sup>14</sup>D. J. Chadi, *Phys. Rev. Lett.* **59**, 1691 (1987).

<sup>15</sup>The Ge surface energy for a  $(001)$   $(2\times 1)$  reconstruction is approximately 0.07 eV/atom lower than for Si [P. C. Kelires and J. Tersoff, *Phys. Rev. Lett.* **63**, 1164 (1989)]. The difference in energy between Si and Ge dimer bonds is  $\sim 0.5$  eV [S. Ciraci and I. P. Batra, *Phys. Rev. B* **38**, 1835 (1988)]. The energy difference between unsaturated Si and Ge bonds is therefore  $(2\times 0.07 + 0.5)/2 = 0.32$  eV. This particular exchange is likely to be enhanced kinetically by the high lattice strain of the rebonded edge configuration. The replacement of a Ge homopolar bond with a Si-Ge heteropolar bond saves an additional 0.13 eV [J. L. Martins and A. Zunger, *Phys. Rev. Lett.* **56**, 1400 (1986)].

<sup>16</sup>Note, we have only considered a subset of all possible phases. Beyond stage (f) in Fig. 2, the number of possible structures diverges rapidly since the ordering may propagate, terminate, or reverse during each successive monolayer growth step.

<sup>17</sup>S. S. Iyer *et al.*, *Appl. Phys. Lett.* **54**, 219 (1989).

<sup>18</sup>Similar considerations predict long-range-ordered structures resulting from alloy deposition at high growth temperatures where monolayer step flow prevails. This provides an alternative explanation to the surface-site-selectivity and surface-stress-induced alloy-ordering mechanisms, respectively, proposed in Ref. 10 and by F. K. LeGoues *et al.*, *Phys. Rev. Lett.* **64**, 2038 (1990).

<sup>19</sup>LeGoues *et al.*, Ref. 18.

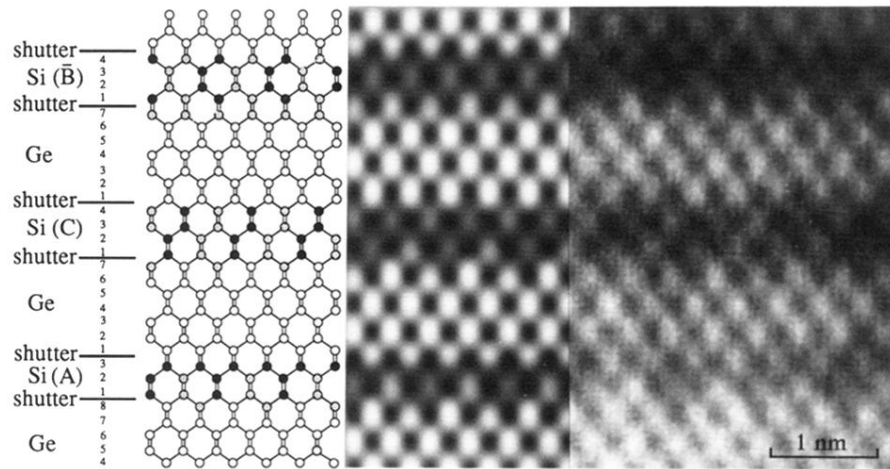


FIG. 1. [110] Z-contrast STEM image of a nominal  $(\text{Si}_4\text{Ge}_8)_{24}$  superlattice showing interfacial ordering. The [001] growth direction is toward the top of the image with the sample thickness increasing toward the lower left-hand corner. Our interpretation of the superlattice structure based on the image simulation indicates the sequential deposition of Si and Ge layers together with the ordered structures  $\bar{B}$ , C, and A resulting from the atom pump mechanism. Open circles represent Ge columns; solid circles, Si columns; and shaded circles, alloy columns. Simulation parameters are  $C_s = 1.3$  mm, convergence angle = 10.3 mrad, and defocus = -69.4 nm.